Journal of Materials Science: Materials in Electronics (2019) 30:5902–5910
https://doi.org/10.1007/s10854-019-00888-y

# Glass structure, crystallization kinetics and dielectric properties of $CeO_2$-added $CaO–B_2O_3–SiO_2$ glass system

Jiao Han[1] · Yao Xiang[1] · Zhiqiang Yao[1] · Yiming Zeng[1] · Peijia Bai[1] · Yunbo Jiang[1] · Wen Chen[1]

Received: 7 November 2018 / Accepted: 4 February 2019 / Published online: 12 February 2019


**Abstract**
This work investigated the effects of $CeO_2$ contents on structure, crystallization behavior and dielectric properties of $CaO–B_2O_3–SiO_2$ glass composition. The MAS-NMR results showed that B occurred as $B^{IIIa}$, $B^{IIIs}$ and $B^{IV}$ species and Si presented as $Q^2$, $Q^3$ and $Q^4$ units in the glasses. As the increase of $CeO_2$ content, the relative amounts of $B^{IV}$ and $B^{IIIs}$ unit decreased while the $B^{IIIa}$ units increased, and the amounts of $Q^4$ and $Q^2$ units increased while the $Q^3$ unit decreased. With increasing $CeO_2$ content, the value of $T_g$ decreased from 743 °C to 717 °C, the activation energy for $CaSiO_3$ first increased and then decreased. For glass–ceramics samples sintered at 825 °C, all samples had the crystalline phases of $CaSiO_3$, $CaB_2O_4$, $Ca_2SiO_4$. In addition, the samples with $CeO_2$ content more than 1 mol% had $CeO_{1.695}$ phase, which changed to be the main crystalline phase when the content of $CeO_2$ increased up to 10 mol%. The $\varepsilon_r$ of the glass–ceramic samples with $CeO_2$ content $x \leq 6$ showed an ascend trend in total, and decreased sharply to 4.1 for the sample with $x = 10$. However, the dielectric loss tan δ would not change significantly with the increasing of $CeO_2$ content. The samples with 1 mol% $CeO_2$ sintered at 825 °C owned $\varepsilon_r$ of 5.4, tan δ of $0.9 \times 10^{-3}$, and CTE of $7.8 \times 10^{-6}$/K. The results indicated that $CaO–B_2O_3–SiO_2$ with $CeO_2$ glass–ceramics could be a potential LTCC substrate material.

## 1 Introduction

Nowadays, miniaturization and integration development of electronic components have set a higher demand for the substrates, which should satisfy the high propagation speed, high wiring density and large chip packaging [1, 2]. The substrate materials of low temperature co-fired ceramic (LTCC) technology should possess low dielectric constant and loss, low coefficient of thermal expansion (CTE) to match with silicon ($3 \times 10^{-6}$/K) and low sintering temperature (< 900 °C) for co-firing with metal electrodes such as Cu, Ag and Au [2, 3]. Among the multiple glass systems utilized in LTCC technology, $CaO–B_2O_3–SiO_2$ glasses take up a crucial position due to its complete sintering properties at temperatures below 900 °C with low dielectric constant ($\varepsilon_r < 6.5$) and dielectric loss (tan $\delta < 1 \times 10^{-3}$) [4, 5] along the last decades.

However, $CaO–B_2O_3–SiO_2$ glasses also exhibit some unfavorable characteristics for the development of future high frequency communication. Their relatively low mechanical strength, narrow sintering window and dielectric properties will hinder their sufficient use in LTCC technological area. In order to satisfy a high level of need of the technical applications, the optimization in preparation method, composition and structure of $CaO–B_2O_3–SiO_2$ glasses is carried out to achieve the required properties [6, 7]. Xia et al. [8] developed a high-performance film for LTCC application through using a kind of silane coupling agent (SCA) to modify the $CaO–B_2O_3–SiO_2$ glass–ceramic powders in tape casting process. The experimental results revealed that the powders modified by SCA with 1.5 wt% additions owned the optimal performance of film, possessing the highest density and best microwave properties of sintered body: the density of sintered body was 2.48 g/cm$^3$, the dielectric constant and dielectric loss were $\varepsilon_r = 5.93$, tan $\delta = 8 \times 10^{-4}$ at 12 Hz. Lee et al. [9] investigated carbon nanotube/graphene oxide-added $CaO–B_2O_3–SiO_2$ glass/$Al_2O_3$ composite. The results showed that the $CaO–B_2O_3–SiO_2$ glass/40 wt% $Al_2O_3$

✉ Jiao Han
hanjiao90@sina.com

✉ Yiming Zeng
zengym0871@126.com

[1] State Key Laboratory of Advanced Technologies for Comprehensive Utilization of Platinum Metals, Kunming Institute of Precious Metals, Kunming 650106, People's Republic of China

composite containing 0.25 wt% graphene oxide and 0.75 wt% carbon nanotube, sintered at 900 °C and subsequently annealed at 850 °C, exhibited a high bending strength of 420 MPa and thermal conductivity of 5.51 W/(mK). These outstanding properties make this composite suitable as a substrate for chip-type supercapacitors.

Moreover, some oxides, such as ZnO [10, 11], MgO [12], $ZrO_2$ [13] and $Al_2O_3$ [14, 15], were introduced into $CaO–B_2O_3–SiO_2$ glass to modify the structure of glass to achieve the required physical, mechanical and dielectric properties. Park et al. [16] studied $50CaO·20ZnO·20B_2O_3·10SiO_2$ glass, which had CTE of $12.8\times10^{-6}$/K and dielectric constant of 13.5. The results indicated the feasibility of the developed glass for the application to LTCC materials with high CTE. Liu et al. [15] prepared $CaO–B_2O_3–SiO_2$ glass ceramics sample with 5 wt% $Al_2O_3$, possessing the best sintering characterization and dielectric properties ($\varepsilon_r\approx7$, $\tan\delta=1.9\times10^{-3}$ at 1 MHz), which was proposed to be suitable for LTCC application. According to our previous report [17], the $CaO–B_2O_3–SiO_2$ glasses with addition of 5 wt% $La_2O_3$ had the best dielectric properties ($\varepsilon_r\approx4.1$, $\tan\delta\approx1.7\times10^{-3}$ at 15 GHz), which exhibited the great potential of rare-earth doping to improve the properties of $CaO–B_2O_3–SiO_2$ systems. In addition, it was interesting that the addition of $CeO_2$ could significantly change the crystallization behavior and microwave dielectric properties of glass–ceramic [18–20]. Liu et al. [20] reported the effect of $CeO_2$ on the $SrO–BaO–Nb_2O_5–B_2O_3–SiO_2$ glass–ceramics, which showed the addition of $CeO_2$ decreased the activation energy of crystallization and enhanced the dielectric constant as well as breakdown strength remarkably.

However, the effects of $CeO_2$ on crystallization behavior and dielectric properties of $CaO–B_2O_3–SiO_2$ glass system have not been taken seriously. In this work, we systematically investigated the effects of $CeO_2$ on glass structure, crystallization behavior, sintering behavior and dielectric properties of $CaO–B_2O_3–SiO_2$ glasses, expecting to develop an optimized material with outstanding dielectric properties for further LTCC application.

## 2 Experimental

### 2.1 Preparation of glass powders

The $(100-x)[40CaO–37SiO_2–23H_3BO_3]+xCeO_2$ glasses, where $x=0$, 0.5, 1, 3, 6 and 10 mol% (noted as C0, C0.5, C1, C3, C6, and C10, respectively) were prepared using AR grade $CaCO_3$, $H_3BO_3$, $SiO_2$, and $CeO_2$ as the starting materials. The glass powders were prepared via a water quenching method as reported in our previous work [14].

### 2.2 Preparation of glass–ceramic samples

The glass powder was granulated with a 4 wt% polyvinyl alcohol (PVA) solution and compacted into disk-shaped specimens under the uniaxial pressure of about 100 MPa. Then the samples were sintered for 20 min in air at temperature ranging from 750 °C to 850 °C with a heating rate of 5°C/min.

### 2.3 Characterization of the samples

The X-ray diffraction XRD (XRD, DMX-2200, Rigaku, Tokyo, JP) of glass powders and glass–ceramic samples was measured using a standard diffractometer with Cu Kα radiation ($\lambda=1.54$ Å) as an X-ray source. All samples were scanned from 10° to 80° at step width of 0.02°. $^{11}B$ and $^{29}Si$ magic angle spinning nuclear magnetic resonance spectroscopy (MAS-NMR, Varian Infinity-plus 400, US) were applied to analyze the structure of B and Si units in glass system. The samples C0, C0.5, C3 and C10 were selected to display the structure change of B and Si with increasing of $CeO_2$ content. The measure condition refers to a reference [21].

The Fourier transform infrared spectra (FT-IR) of the glasses were recorded at room temperature using the KBr technique by a Thermo Nicolet Smart-380 FT-IR spectrometer in a wave number region between 400 and 2000 $cm^{-1}$ with a resolution of 2 $cm^{-1}$.

To determine the glass transition temperature and the crystallization kinetics of the glasses, a differential scanning calorimetry (DSC, STA409 PG/PC, Netzsch, Germany) were carried out in air from room temperature to 1000 °C with heating rates of 5, 10, 15 and 20 °C/min with a reference material of α-alumina powders.

The densities of glass–ceramic samples were measured by the Archimedes method. The surface morphologies of glass–ceramic samples were studied using a field emission scanning electron microscope (Ultra 55, ZEISS). The surface of samples was eroded 60 s using 2% HF solution. The network analyzer (N5230C, Agilent) was utilized to measure the dielectric properties of all samples at 15 GHz. The coefficient of thermal expansion (CTE) of all samples was carried out in argon atmosphere from 25 to 500 °C with heating rates of 5°C/min by a thermal expansion analyzer (DL 402, Netzsch).

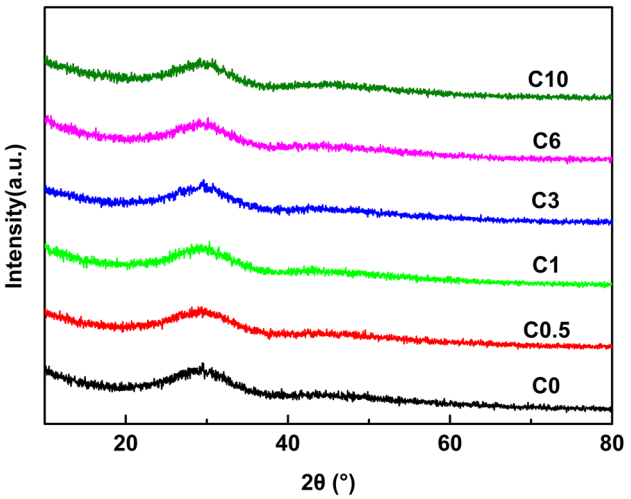


**Fig. 1** X-ray diffraction patterns of all glass samples

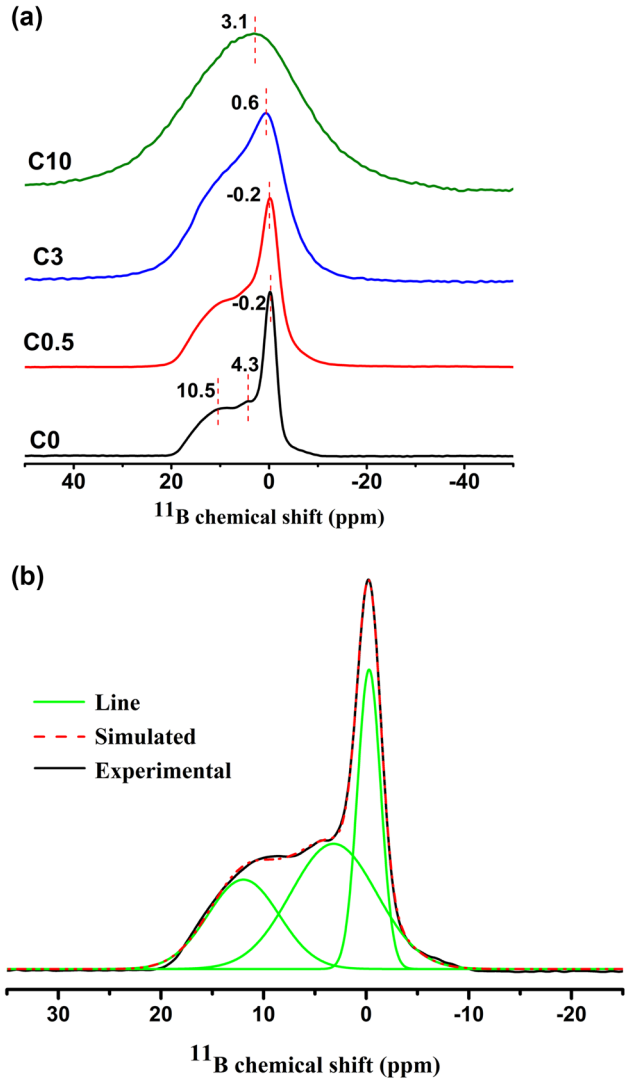


**Fig. 2** $^{11}$B MAS-NMR spectra of C0, C0.5, C3 and C10 (**a**) and deconvolution spectra of C0 (**b**)

## 3 Results and discussion

The XRD patterns of all glass samples are presented in Fig. 1. According to the experimental results, the diffraction peak curves, without crystalline peaks, indicated the amorphous state and good glass forming ability of all samples.

The $^{11}$B MAS-NMR spectra of C0, C0.5, C3 and C10 samples are shown in Fig. 2a. For sample C0, it is worth noting that two relatively broad peaks centered at 4.3 ppm and 10.5 ppm, which are associated with asymmetric boron units ($B^{IIIa}$, boron connected with 1 or 2 bridging oxygens) and symmetric trigonal boron units ($B^{IIIs}$, boron connected with 0 or 3 bridging oxygens) [14, 22, 23], respectively. The sharper peak located at −0.2 ppm could be assigned to tetrahedral ($BO_4$, $B^{IV}$) boron species, which is danburite like structural units of boron where each tetrahedral boron is coordinated with one boron atom and three Si tetrahedrons [$B(OB)(OSi)_3$] [14, 23]. By performing $CeO_2$ addition, the peak shifts to higher values of the chemical shifts i.e. from −0.2 to 3.1 ppm for x = 0 and x = 10, respectively. In order to quantify the relative amounts of $B^{IIIa}$, $B^{IIIs}$ and $B^{IV}$ units of boron in glasses, the $^{11}$B MAS-NMR spectra were deconvoluted and an example of C0 was presented in Fig. 2b. The NMR parameters, the isotropic chemical shift ($\delta_{iso}$) and the amount of boron structure units were listed in Table 1. The relative amount of $B^{IV}$ units decreases from 29% to 8% and $B^{IIIs}$ is from 26% to 20% then disappears, while the amount of $B^{IIIa}$ units increases from 45% to 92% with the increasing of $CeO_2$ content (Table 1).

Figure 3a reveals the $^{29}$Si MAS-NMR spectra of C0, C0.5, C3 and C10 samples. It can be noted that for all glass samples, the spectra present a peak maximum near −84 ppm. Deconvolution of $^{29}$Si spectra was performed using Gaussian to quantitatively clarify the fractions and distribution of different Si units in glasses. An example of C0 was presented in Fig. 3b, the isotropic chemical shifts ($\delta_{iso}$) and the relative amounts of different Si units were listed in Table 1. The peaks for all glasses around −82 ppm, −87 ppm and −109 ppm, which are characteristic of the $Q^2$, $Q^3$ and $Q^4$ structural units of silicon, respectively [24]. With the increasing of $CeO_2$, the amount of $Q^4$ unit increases from 0% to 36% and the $Q^2$ increases from 25% to 50%, while the amount of $Q^3$ unit decreases from 75% to 14%.

The MAS-NMR results had shown that B occurred as $B^{IIIa}$, $B^{IIIs}$ and $B^{IV}$ (1B,3Si) species and Si presented as $Q^2$, $Q^3$ and $Q^4$ units in the glasses. As the increase of $CeO_2$ content, the relative amount of $B^{IV}$ and $B^{IIIs}$ units decreased while the amount of $B^{IIIa}$ units increased, and the amount of $Q^4$ and $Q^2$ unit increased while the amount

**Table 1** NMR parameters for $^{11}B$ and $^{29}Si$ deconvolution

| | $^{11}B$ | | | $^{29}Si$ | | |
|---|---|---|---|---|---|---|
| | Boron site | $\delta_{iso}$ (ppm) | Amount(%) | Silicon units | $\delta_{iso}$ (ppm) | Amount(%) |
| C0 | $B^{IIIa}$ | 3.3 | 45 | $Q^2$ | −82.8 | 25 |
| | $B^{IIIs}$ | 12.1 | 26 | $Q^3$ | −86.3 | 75 |
| | $B^{IV}$(1B,3Si) | −0.3 | 29 | $Q^4$ | – | – |
| C0.5 | $B^{IIIa}$ | 2.9 | 59 | $Q^2$ | −82.7 | 35 |
| | $B^{IIIs}$ | 12.5 | 20 | $Q^3$ | −86.5 | 61 |
| | $B^{IV}$(1B,3Si) | −0.3 | 21 | $Q^4$ | −109.0 | 4 |
| C3 | $B^{IIIa}$ | 6.1 | 81 | $Q^2$ | −82.5 | 35 |
| | $B^{IIIs}$ | – | – | $Q^3$ | −87.9 | 49 |
| | $B^{IV}$(1B,3Si) | −0.1 | 19 | $Q^4$ | −108.9 | 16 |
| C10 | $B^{IIIa}$ | 5.4 | 92 | $Q^2$ | −82.5 | 50 |
| | $B^{IIIs}$ | – | – | $Q^3$ | −88.1 | 14 |
| | $B^{IV}$(1B,3Si) | 1.1 | 8 | $Q^4$ | −108.5 | 36 |

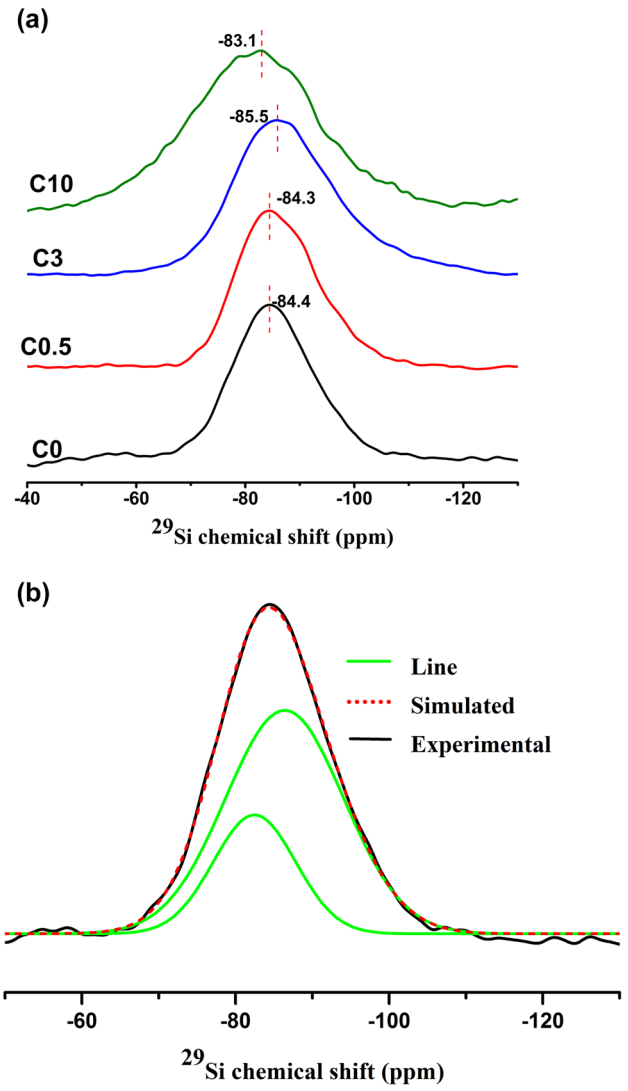


**Fig. 3** $^{29}Si$ MAS-NMR spectra of C0, C0.5, C3 and C10 (**a**) and deconvolution spectra of C0 (**b**)

of $Q^3$ units decreased. The change of boron species could be ascribed to the $CeO_2$ in glass system. Generally, the six or eight coordination numbers and ionic field strength of 0.83 [25] make cerium play the part of network modifier in the glass system, and it prefers to bridge $BO_3$ units rather than form $BO_4$ groups [26]. This will make the amount of $BO_3$ units increase. Moreover, cerium oxide is considered to form Ce–O–B(3) bonds at the expense of the bridging B(3)–O–B(3) bonds [26], which leads to the increase of $B^{IIIa}$ and the decrease of $B^{IIIs}$. Additionally, according to our previous study [14], the $B^{IV}$ species can resolve into symmetric $BO_3$ species and non-bridging oxygen (NBO), the $B^{IIIs}$ species with the NBO can form $B^{IIIa}$ species, both of which resulting in the change of boron structural units. On the other hand, the non-bridging oxygen created by $B^{IV}$ resolving and $[CeO_6]$ or $[CeO_8]$ unit forming [20] in the glass may react with $Q^n$ to form a $Q^{n-1}$ species. The structure of $Q^4$ unit is most stable among all $[SiO_4]$ tetrahedrons so that it is difficult to react with NBO to form $Q^3$ unit [17]. But the existing $Q^3$ unit will react with NBO to generate $Q^2$ unit, which make the amount of $Q^2$ unit increase. Furthermore, the added $CeO_2$ in glass will release a lot of free oxygen, which will occur in the formation of Si–O link to cause sectional $Q^3$ unit turning into $Q^4$ unit. Therefore, the amount of $Q^4$ and $Q^2$ unit increased while the amount of $Q^3$ units decreased with the increasing of $CeO_2$ content.

Figure 4 displays the FT-IR spectra between 400 and 2000 $cm^{-1}$ for of all glasses. As it shown, the broad bands confirmed the amorphous nature (as shown in Fig. 1) and wide distribution of $Q^n$ units in glass systems. Seven absorption bands were observed in all glasses. Their peak positions and intensity are related to the $CeO_2$ contents obviously. The assignments are shown in Table 2. The band located at 1427 $cm^{-1}$ shifted to lower wavenumber obviously with the increasing of $CeO_2$ content, the wavenumber locations were separately 1427, 1412, 1407, 1404, 1402, 1400 $cm^{-1}$ from

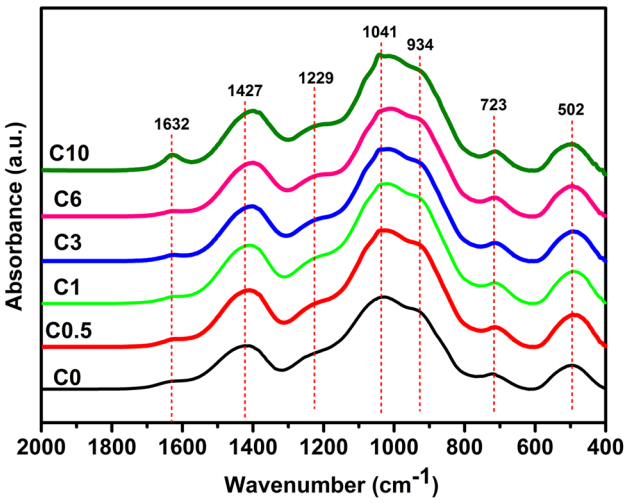


**Fig. 4** The FT-IR spectra of the glasses

x = 0 to x = 10, respectively. In addition, the peak located at 1041 $cm^{-1}$ became sharper with the increase of $CeO_2$. In addition, new band didn't appear with the increasing of $CeO_2$ content, indicated that the $CeO_2$ may only play the part of network modifier in $CaO–B_2O_3–SiO_2$ glasses.

Figure 5a presents the DSC plots of all the glasses measured at $\beta = 5$°C/min. For all samples, the curves showed 2 crystallization peaks ($T_{P1}$ and $T_{P2}$), related to the formation of the crystalline phase of wollastonite [32] and borocalcite [33], respectively. The values of glass transition temperature $T_g$, which obtained from the onset of slope change of the DSC curves, and $T_{P1}$, $T_{P2}$ for all glasses were listed in Table 3. With increasing $CeO_2$ content, the value of $T_g$ decreased from 743 °C to 717 °C. This could be ascribed to the free oxygen, which brought by $CeO_2$ addition, destroyed the glass network structure and impaired the glass network polymerization degree. The exothermic peak temperatures $T_{P1}$ of glasses first increased and then decreased obviously with the increasing of $CeO_2$ content. It meant that a little bit of $CeO_2$ addition could make $CaSiO_3$ crystallization difficult, but this system would be easier to crystallize when the addition of $CeO_2$ content exceeded 3 mol%. In addition, the $T_{P2}$ increased obviously with the increasing of $CeO_2$ content, which showed that the $CeO_2$ inhibited the crystallization of $CaB_2O_4$. The DSC curves at $\beta = 10$, 15, 20 °C/min were also measured (the crystallization exothermal peak temperatures are listed in Table 3) in order to analyze the crystallization kinetics of glasses, which can be described by the expression [20]:

$$\ln \frac{\beta}{T_P^2} = -\frac{E}{RT_P} + constant \quad (1)$$

where $T_p$ is the crystallization peak temperature in a DSC curve, $\beta$ is the heating rate of DSC, R is the gas constant, and $E$ is the activation energy for crystallization. According to the equation, a plot of $(\beta/T_{p1}^2)$ versus $1/T_{p1}$ yields a straight line in which the slopes are proportional to the activation energy of crystallization. These plots are shown in Fig. 5b and the values of crystallization activation energy for $CaSiO_3$ are shown in Table 3. It was found that the activation energy first increased and then decreased with the increasing $CeO_2$ content, which conformed to the change rule of $T_{P1}$. The change of crystallization activation energy may be attributed to the $Q^n$ variation in glass structure.

Figure 6a–c show the XRD patterns of all glass–ceramics samples sintered at 750 °C, 775 °C and 825 °C for 20 min, respectively. For samples sintered at 750 °C (as shown in Fig. 6a), it could be observed that C0 sample remained the glassy state and samples with $CeO_2$ content occur a slight crystallization phenomenon. The samples C0.5, C1 and C3 only had a bit of $CaSiO_3$ phase (PDF standard card: 00-003-0626), while the $CeO_{1.695}$ phase (PDF standard card: 01-089-8429) started to appear in samples C6 and C10. For glass–ceramics samples sintered at 775 °C (as shown in Fig. 6b), all samples had $CaSiO_3$ phase. With the increase of $CeO_2$ content, the intensity of $CeO_{1.695}$ diffraction peak

**Table 2** The FT-IR vibrational bands and their assignments of all glasses

| Wavenumber($cm^{-1}$) | | | | | | Assignments | References |
|---|---|---|---|---|---|---|---|
| C0 | C0.5 | C1 | C3 | C6 | C10 | | |
| 502 | 501 | 501 | 505 | 503 | 499 | Bending vibration of Si–O–Si bonds in [$SiO_4$] tetrahedron | [27] |
| 723 | 721 | 721 | 721 | 721 | 721 | Bending vibration of the B–O–B bonds | [14, 26] |
| 934 | 933 | 933 | 932 | 932 | 932 | B–O stretching in $BO_4$ units | [28] |
| 1041 | 1042 | 1043 | 1045 | 1047 | 1050 | Asymmetric stretching vibration of Si–O–Si in [$SiO_4$] tetrahedron unit ($Q^2$)<br>B–O asymmetric stretching of [$BO_4$] unit | [10, 29, 30] |
| 1229 | 1226 | 1220 | 1217 | 1214 | 1210 | (B–O)asym bonds from orthoborate groups | [6, 31] |
| 1427 | 1412 | 1407 | 1404 | 1402 | 1400 | Antisymmetric stretching vibration of [$BO_3$] | [31] |
| 1632 | 1632 | 1632 | 1632 | 1632 | 1632 | The H–O vibration of $H_2O$ | [29] |

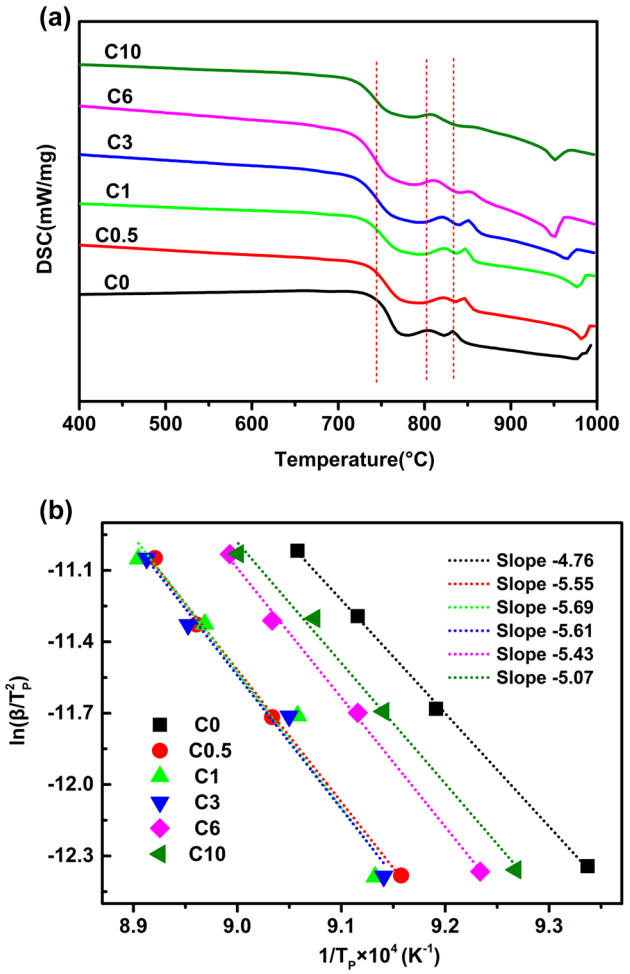


**Fig. 5** DSC curve of the studied glasses at $\beta = 5$°C/min (**a**) and plots of ln ($\beta/T_{p1}^2$) versus $1/T_{p1}$ (**b**)

gradually increased, which was accompanied by a decrease in $CaSiO_3$. When the content of $CeO_2$ increased to 10 mol%, the main crystalline phase changed to be $CeO_{1.695}$. For glass–ceramics samples sintered at 825 °C (as shown in Fig. 6c), all samples had crystalline phases of $CaSiO_3$, $CaB_2O_4$ (PDF standard card: 00-001-0833), $Ca_2SiO_4$ (PDF standard card: 01-087-1259). In addition, the samples with $CeO_2$ content more than 1 mol% had $CeO_{1.695}$ phase, which changed to be the main crystalline phase when the content of $CeO_2$ increased to 10 mol%. Figure 6d shows the XRD patterns of sample with 1 mol% $CeO_2$ addition sintered at different temperatures. The sample sintered at 750 °C was amorphous. After calcination of glass–ceramic at 775 °C, $CaSiO_3$ phase as the main phase was observed. When the temperature was above 800 °C, a couple of minor XRD peaks for $CaB_2O_4$ were also detected. The XRD patterns of the glass–ceramics samples sintered at 800 °C and 850 °C (not shown here) had the similar change rule with samples sintered at 775 °C and 825 °C respectively, indicating that all samples will gradually crystallize with the increasing of sintering temperature and achieve the complete crystallization at 825 °C.

The values of the bulk density of the glass–ceramics samples sintered at different temperatures are depicted in Fig. 7. The densities of all samples first decreased with the increasing sintering temperature and then remained about the same when sintering temperature was above 800 °C. This is because all the samples have been completely crystallization and reach a steady state when the sintering temperature is up to 825 °C. The results are in accordance with previous outcome revealed in XRD. With the increase of $CeO_2$ content, the densities of the samples (Table 3) sintered at 825 °C first increased slowly from 2.4 g/cm$^3$ to 2.7 g/cm$^3$ when the $CeO_2$ content increase from 0 to 6 mol%, and then dropped dramatically to 1.8 g/cm$^3$ when the content of $CeO_2$ increased to 10 mol%. Considering the results of XRD and densities, the optimum sintering temperature of glass–ceramics samples was 825 °C.

Figure 8 displays the SEM micrographs of the surface of the glass–ceramics samples sintered at 825 °C for 20 min with different $CeO_2$ contents. It was observed that the all glass–ceramics samples were mainly composed of the crystal phase (spherical particles) and the glass phase. For C0 to C3 samples, the amounts of spherical particles, which mainly corresponded to $CaSiO_3$ phase (as shown in Fig. 6c), decreased obviously. This result is consistent with DSC data

**Table 3** Characteristic temperatures and physical properties for all glasses

| | $T_g$ (°C) | $T_p$ at different heating rates (°C) | | | | | | | | $E$ ($T_{P1}$) (kJ/mol) | CTE ($\times 10^{-6}$/K) |
|---|---|---|---|---|---|---|---|---|---|---|---|
| | | 5 °C/min | | 10 °C/min | | 15 °C/min | | 20 °C/min | | | |
| | | $T_{P1}$ | $T_{P2}$ | $T_{P1}$ | $T_{P2}$ | $T_{P1}$ | $T_{P2}$ | $T_{P1}$ | $T_{P2}$ | | |
| C0 | 743 | 798 | 832 | 815 | 839 | 824 | 852 | 831 | 865 | 395.7 | 7.6 |
| C0.5 | 732 | 819 | 846 | 834 | 863 | 843 | 875 | 848 | 889 | 461.4 | 7.9 |
| C1 | 727 | 822 | 847 | 831 | 864 | 842 | 882 | 850 | 899 | 473.1 | 7.8 |
| C3 | 721 | 821 | 851 | 832 | 870 | 844 | 893 | 849 | 907 | 466.4 | 8.0 |
| C6 | 717 | 810 | 852 | 824 | 879 | 834 | 901 | 839 | – | 451.5 | 7.8 |
| C10 | 717 | 806 | 857 | 821 | 880 | 829 | – | 838 | – | 421.5 | 7.9 |

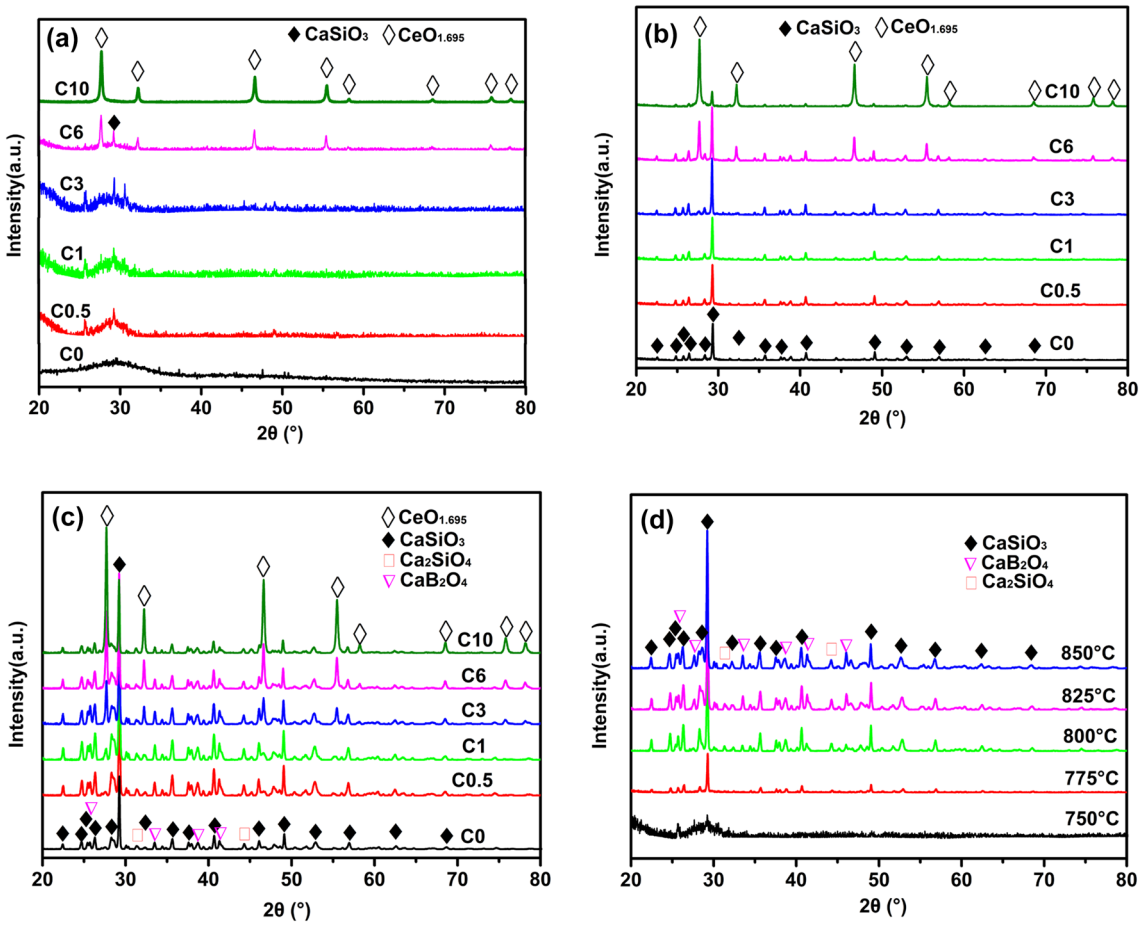


**Fig. 6** X-ray diffraction patterns of glass–ceramics samples sintered at **a** 750 °C, **b** 775 °C, **c** 825 °C and **d** sample with 1 mol% $CeO_2$ addition sintered at different temperatures

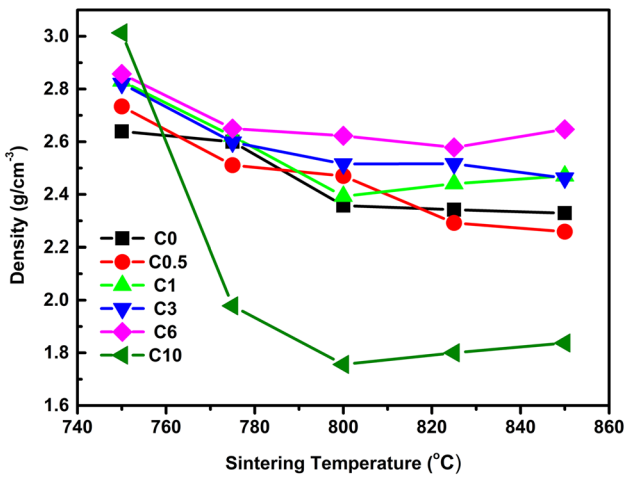


**Fig. 7** Densities of glass–ceramics samples sintered at different temperatures

where the values of the activation energy increase from C0 to C3 gradually. In addition, the uniform and dense microstructure with grain sizes around 500 nm could be observed in samples C0, C0.5 and C1. With the further increase of $CeO_2$ contents, $CeO_2$ deteriorated the uniform microstructure (as shown in C3), which had the smallest grain size approaching 100 nm and the largest grain size ~ 700 nm. For C6 sample, the grain size greatly decreased to < 100 nm and the amount of grains increased significantly. Upon the addition of 10 mol% $CeO_2$, the grain size kept growing and had the average grain size about 200 nm, with the smallest grain size < 100 nm and the largest grain size ~ 400 μm. Based on the results of XRD (Fig. 6c), the grains in C6 and C10 mainly are $CeO_{1.695}$ phase.

The microwave dielectric properties of the glass–ceramics sintered at 825 °C as a function of the $CeO_2$ content are presented in Fig. 9. It was noticed that $\varepsilon_r$ of the glass–ceramic samples with $CeO_2$ content $x \leq 6$ showed an ascend trend in total, and decreased sharply to 4.1 for the sample with $x = 10$, probably owing to its low density. For sample C10, the excess $Ce^{4+}$, as the network modifier in

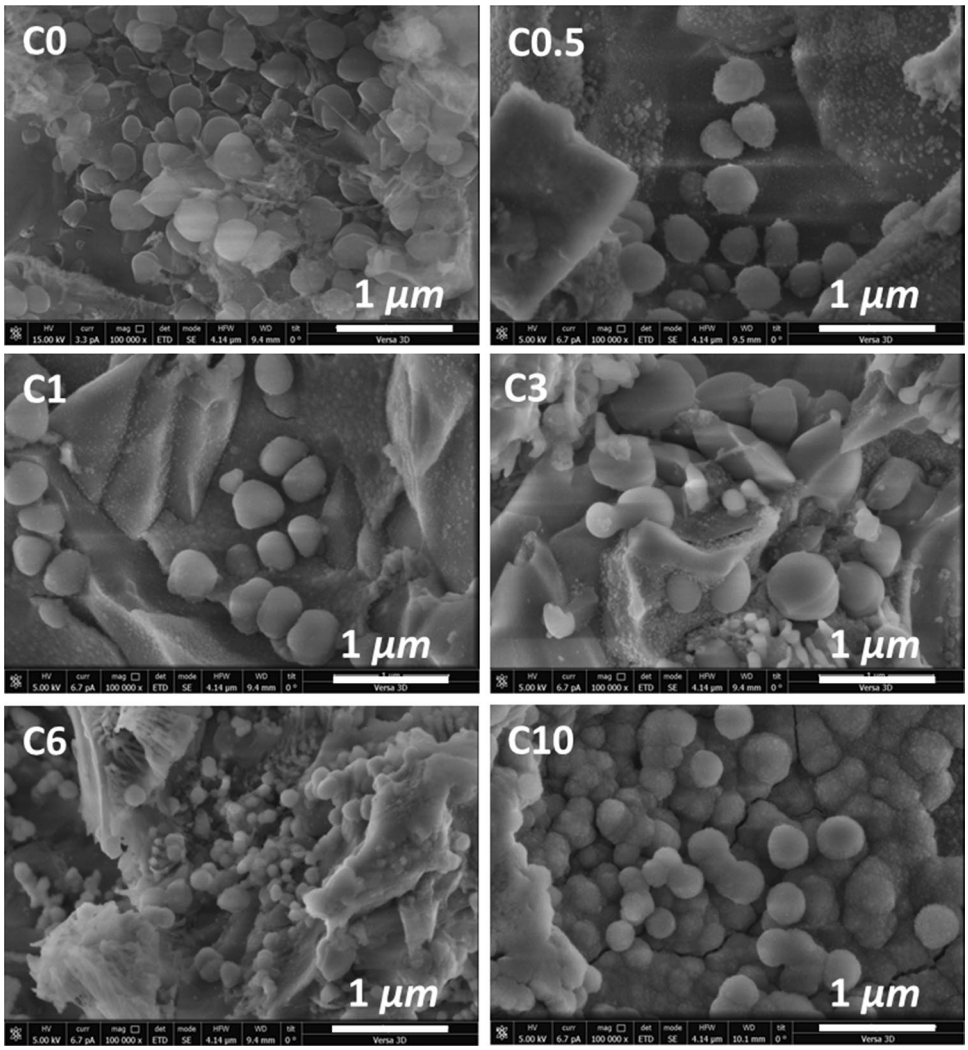


**Fig. 8** SEM photographs of the surface of the glass–ceramics sintered at 825 °C with different $CeO_2$ contents

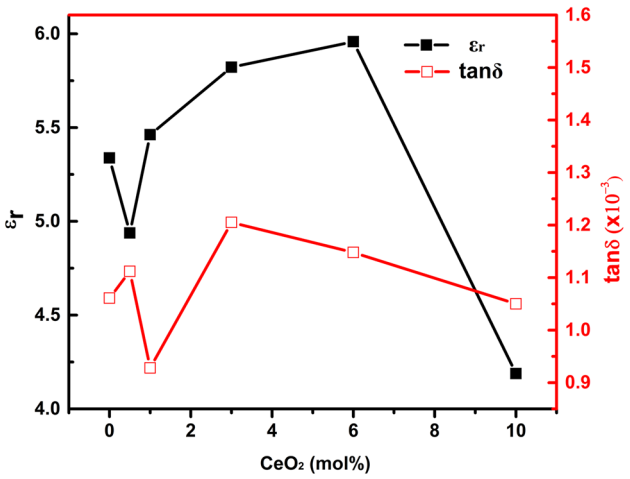


**Fig. 9** The microwave dielectric properties of glass–ceramic samples sintered at 825 °C as a function of the $CeO_2$ content

the glass network, made the massive formation of $CeO_{1.695}$ phase in the glass systems. This would greatly deteriorate the dielectric properties. However, the dielectric loss tan δ will not change significantly with the increasing of $CeO_2$ content, within a small scope of $0.9–1.2\times10^{-3}$. The results reveal that the dielectric properties of the glass–ceramics are closely related to density and microstructure. In addition, the coefficients of thermal expansion (CTE) averaging from 25 °C to 500 °C for glass–ceramic samples sintered at 825 °C are listed in Table 3. The CTE of the glass–ceramic samples with $CeO_2$ content had slightly difference compared to the value $7.6\times10^{-6}$/K of C0.

## 4 Conclusions

In this work, we investigated the structure, crystallization behavior and dielectric properties of $CaO–B_2O_3–SiO_2$ glass with $CeO_2$ addition. The NMR results revealed that the Ce played the network modifier role in $CaO–B_2O_3–SiO_2$

glasses, and B went into the glass network as both fourfold and threefold coordination whereas the Si occurred in the form $Q^2$, $Q^3$ and $Q^4$ units. With the increasing of $CeO_2$ content, the relative amount of $B^{IV}$ and $B^{IIIs}$ units decreased while the amount of $B^{IIIa}$ units increased, and the amount of $Q^4$ and $Q^2$ unit increased while the amount of $Q^3$ units decreased. The addition of $CeO_2$ has been found to decrease $T_g$ from 743 °C to 717 °C. For the glass–ceramics samples sintered at 825 °C, the crystalline phases of C0 were $CaSiO_3$, $CaB_2O_4$, $Ca_2SiO_4$. Upon the addition of $CeO_2$ more than 1 mol%, the $CeO_{1.695}$ phase occurred and changed to be the main crystalline phase when the content of $CeO_2$ increased to 10 mol%. After the analysis and comparison, we could conclude that the C1 sample had the optimum properties ($\varepsilon_r$: 5.4, tan δ: $0.9\times10^{-3}$, CTE: $7.8\times10^{-6}$/K), which indicated the potential application for LTCC substrate.

**Acknowledgements** This work was supported by the fund of the Basic Applied Research Foundation of Yunnan Province (Grant No. 2016FD125, 2016FB083), Key New Product Project of Yunnan Province (Grant No. 2016BA009), Chinese academy of Sciences Key Project (Grant No. KLIFMD201605) and 2017 Kunming Advanced Talent Funding (13020163).

## References

1. Z. Qing, Mater. Lett. **212**, 126 (2018)
2. K. Manu, M.T. Sebastian, Ceram. Int. **42**, 1210 (2016)
3. X. Zhou, E. Li, S. Yang, B. Li, B. Tang, Y. Yuan, S. Zhang, Ceram. Int. **38**, 5551 (2012)
4. H. Zhu, H. Zhou, M. Liu, P. Wei, G. Xu, G. Ning, J. Mater. Sci. Mater. Electron. **20**, 1135 (2008)
5. C.C. Chiang, S.F. Wang, Y.R. Wang, Y.F. Hsu, J. Alloys Compd. **461**, 612 (2008)
6. Y. Lai, Y. Zeng, X. Tang, H. Zhang, J. Han, H. Su, RSC Adv. **6**, 93722 (2016)
7. S.F. Wang, Y.R. Wang, Y.F. Hsu, C.C. Chiang, J. Alloys Compd. **498**, 211 (2010)
8. Y. Xia, Y. Hu, L. Ren, X. Luo, W. Gong, H. Zhou, J. Eur. Ceram. Soc. **38**, 253 (2018)
9. T.H. Lee, S.H. Cho, T.G. Lee, H.T. Kim, I.K. You, S. Nahm, J. Am. Ceram. Soc. **101**, 3156 (2018)
10. J. Han, Y. Lai, Y. Xiang, S. Wu, Y. Xu, Y. Zeng, J. Chen, J. Liu, J. Mater. Sci. Mater. Electron. **28**, 6131 (2017)
11. S. Cetinkaya Colak, I. Akyuz, F. Atay, J. Non-Cryst. Solids **432**, 406 (2016)
12. H. Shao, T. Wang, Q. Zhang, J. Alloys Compd. **484**, 2 (2009)
13. S. Khan, G. Kaur, K. Singh, Ceram. Int. **43**, 722 (2017)
14. J. Han, Y. Lai, Y. Xiang, S. Wu, Y. Zeng, H. Yang, Y. Mao, Y. Yang, RSC Adv. **7**, 14709 (2017)
15. J.Z. Liu, X.F. Wu, N.X. Xu, Q.L. Zhang, H. Yang, J. Mater. Sci. Mater. Electron. **26**, 8899 (2015)
16. J.S. Park, Y. Kim, H. Shin, J.H. Moon, W. Lim, J. Am. Ceram. Soc. **91**, 3630 (2008)
17. Y. Xiang, J. Han, Y. Lai, S. Li, S. Wu, Y. Xu, Y. Zeng, L. Zhou, Z. Huang, J. Mater. Sci. Mater. Electron. **28**, 9911 (2017)
18. J. Wang, W. Chen, L. Luo, J. Alloys Compd. **464**, 440 (2008)
19. S.B. Sohn, S.Y. Choi, J. Non-Cryst. Solids **282**, 221 (2001)
20. T.Y. Liu, G.H. Chen, J. Song, C.I. Yuan, Ceram. Int. **39**, 5553 (2013)
21. S. Sen, Z. Xu, J.F. Stebbins, J. Non-Cryst. Solids **226**, 29 (1998)
22. H.R. Gaddam, J.M.F. Fernandes, Ferreira, RSC Adv. **5**, 41066 (2015)
23. G. Parkinson, D. Holland, M.E. Smith, A.P. Howes, C.R. Scales, J. Phys. Condens. Matter **19**, 415114 (2007)
24. T. Schaller, J.F. Stebbins, M.C. Wilding, J. Non-Cryst. Solids **243**, 146 (1999)
25. M.B. Volf, *Chemical Approach to Glass* (Elsevier, Amsterdam, 1984)
26. G. El-Damrawi, K. El-Egili, Physica B **299**, 180 (2001)
27. G.J. Mohini, N. Krishnamacharyulu, G. Sahaya Baskaran, P.V. Rao, N. Veeraiah, Appl. Surf. Sci. **287**, 46 (2013)
28. R.C. Lucacel, T. Radu, A.S. Tătar, I. Lupan, O. Ponta, V. Simon, J. Non-Cryst. Solids. **404**, 98 (2014)
29. K. Singh, I. Bala, V. Kumar, Ceram. Int. **35**, 3401 (2009)
30. M. Sitarz, J. Non-Cryst. Solids **357**, 1603 (2011)
31. D. Winterstein-Beckmann, D. Möncke, E.I. Palles, L. Kamitsos, Wondraczek, J. Non-Cryst. Solids **405**, 196 (2014)
32. J.H. Jean, C.R. Chang, C.D. Lei, J. Am. Ceram. Soc. **87**, 1244 (2004)
33. C.R. Chang, J.H. Jean, J. Am. Ceram. Soc. **82**, 1725 (1999)